JOURNAL OF AIRCRAFT
Vol. 44, No. 3, May–June 2007

Simplified Rotor Inflow Model for Descent Flight

Chang Chen* and J. V. R. Prasad†
Georgia Institute of Technology, Atlanta, Georgia 30332

DOI: 10.2514/1.25910

A simplified inflow model called the 'ring vortex model' is developed for a rotor in descent condition. The ring vortex model accounts for the flow interaction between rotor wake and surrounding airflow in descent flight by using a series of vortex rings along the rotor wake. Important features of the ring vortex model are illustrated in detail, including the convection speed, the vortex strength, and the number of vortex rings. An augmentation to total mass flow parameter in the existing inflow equation is proposed to create a steady-state transition between the helicopter and the windmill branches. With the ring vortex model, it is feasible to predict rotor inflow over a wide range of descent conditions. Numerical results show good correlation with experimental data for both axial and inclined descent. In addition, the ring vortex model is used to explain the influence of model parameters (such as blade twist and blade taper) on rotor-induced velocity during descent flight.

Nomenclature

C_Q	=	rotor torque coefficient
C_T	=	rotor thrust coefficient
$\overline{C}_T$	=	average rotor thrust coefficient
k_{ring}	=	nondimensional factor used to compute induced velocity from a vortex ring
k_Γ	=	strength factor of a vortex ring
N_b	=	number of blades
N_{ring}	=	number of vortex rings
R	=	rotor radius
T	=	rotor thrust
V_h	=	rotor-induced velocity at hover
V_i	=	rotor-induced velocity
$V_{\text{ver,con}}$	=	vertical convection speed of a vortex ring
V_x	=	rotor horizontal speed (positive forward)
V_z	=	rotor vertical speed (positive in climb)
α	=	angle of descent
Γ	=	strength of a vortex ring
ΔT	=	amplitude of thrust fluctuation with respect to mean value of thrust
ΔV_i	=	increment of rotor-induced velocity due to the presence of vortex rings
η	=	normalized rotor vertical speed (positive in climb)
η_{peak}	=	normalized rotor vertical speed corresponding to the peak value of induced velocity
λ	=	nondimensional total inflow
λ_m	=	nondimensional average induced velocity
$\overline{\lambda}$	=	average total inflow
μ	=	advance ratio
μ_z	=	nondimensional climb rate in the tip path plane
$\bar{\mu}$	=	rotor advance ratio normalized by induced flow at hover
ν	=	normalized induced velocity
ν_{mom}	=	normalized induced velocity from momentum theory at $\eta = \eta_{\text{peak}}$
ν_{peak}	=	peak value of normalized induced velocity in experimental results
$\nu_{\text{ver,con}}$	=	normalized vertical convection speed of a vortex ring
ν_{con}	=	normalized convection speed of a vortex ring
σ_e	=	equivalent rotor solidity
Ω	=	rotor rotational speed

Received 15 June 2006; revision received 16 November 2006; accepted for publication 28 November 2006.

*Doctor of Philosophy, Georgia Institute of Technology; currently Senior Member of Technical Staff, Defence Science Organization National Laboratories, Singapore.

†Professor, School of Aerospace Engineering, Georgia Institute of Technology, 270 Ferst Drive. Associate Fellow AIAA.

Introduction

A HELICOPTER rotor in descent flight encounters its own wake, resulting in a doughnut-shaped ring around the rotor disk, known as the vortex ring state (VRS). As simple momentum theory is no longer valid for a rotor in VRS; modeling of rotor inflow in the VRS continues to daunt researchers, especially for flight simulation applications. Although routine operations of a helicopter in the VRS are restricted, a better understanding of the VRS problem and an ability to accurately predict the VRS boundary provide certain advantages. For example, a detailed understanding of the VRS problem may lead to the development of effective systems for VRS avoidance. Also, the ability to accurately predict the VRS boundary may lead to a better utilization of the safe operational envelope to facilitate significant noise abatement, e.g., through segmented steep approaches for civilian helicopters. Thus, the development of accurate inflow models is warranted for improving the fidelity of rotorcraft flight simulation and for assessment of handling qualities in descent flight.

Typical aerodynamic phenomena associated with VRS include flow unsteadiness, excessive thrust and torque fluctuations, and a significant increase in vibration. Castles and Gray [1] conducted wind tunnel tests with multiple rotor configurations and observed considerable fluctuations in the induced velocity distribution in VRS. Yaggy and Mort [2] indicated reduction in steady-state thrust and large thrust oscillation in descent condition. Washizu et al. [3] conducted experiments to measure unsteady aerodynamic characteristics of a rotor operating in VRS. The VRS boundary was derived based on the magnitude of $\Delta T/T$. Wolkovitch [4] proposed a flow model that consisted of a slipstream with uniform flow surrounded by a protective tube of vorticity. The flow model was used to predict thrust fluctuations in VRS and good agreement with measured thrust fluctuations were found [3,5]. Empey and Ormiston [6] tested a one-eighth scale AH-1G helicopter in a wind tunnel. Significant thrust oscillations were shown in descent conditions. Wang [7] applied the classical vortex theory in axial descent with a linear decay of circulation of trailing vortices owing to the effect of fluid viscosity and interaction of induced flow with opposite freestream flow. The resultant induced velocity curve from Wang's model matched well with experimental data from [1]. Xin and Gao [8,9] carried out whirling beam tests in both axial and nonaxial descent conditions.

From the tests, VRS boundary was obtained based on the experimental measurements of rotor torque fluctuations. Leishman et al. [10] applied the free-vortex method in the VRS study. The onset and development of the VRS was viewed as the result of spatial and temporal wake instability. Brown et al. [11] developed a vorticity transport model in the investigation of blade twist effect on rotor in VRS. It was found that a blade with high twist was more prone to develop wake instability.

Dynamic behaviors of a full-scale helicopter operating in VRS condition include uncommanded drop in descent rate, an increase in required power, and loss of control effectiveness. Basset and Prasad [12] explored the use of nonlinear analysis tools such as the bifurcation method in gaining an understanding of the flow dynamics associated with the VRS. Taghizad et al. [13] conducted flight tests using a Dauphin helicopter. The test program identified the main characteristics in VRS condition as a sudden increase in descent rate. The VRS effect was not observed beyond $V_x/V_h = 1$. Brand et al. [14,15] conducted an extensive flight test program to evaluate VRS effects on the V-22 tilt-rotor aircraft. Uncommanded thrust fluctuations and uncommanded roll response were recommended as two criteria in defining VRS boundary for the V-22.

Momentum theory has been successfully used for rotor inflow modeling in hover, climb, and forward flight conditions. However, momentum theory breaks down in descent flight due to the collapse of a smooth slipstream. Nevertheless, researchers have developed various methods in extending momentum theory for descent flight. One of the earliest efforts can be traced back to Glauert [16]. Recent attempts were from He et al. [17] and Taghizad et al. [13]. They individually formulated parametric extensions of momentum theory in the flow model to remove the modeling singularity in VRS and rendered simulation models covering the full range of flight conditions. Perhaps the most comprehensive parametric extension of momentum theory was from Johnson [18]. A broad review of available wind tunnel and flight test data was conducted. Based on the available data, a VRS inflow model was developed suitable for simple calculations and for real-time simulations. Using the developed VRS model, Johnson showed negative (unstable) heave damping for a certain range of descent rates and the VRS boundary was thus defined in terms of the stability boundary of the vehicle flight dynamics. However, models based on parametric extension of momentum theory lack dependence on critical rotor parameters such as rotor solidity, blade twist, etc., and hence, they may not be very useful for their applications in flight simulations at the design stage of a helicopter.

In this paper, a simplified model of inflow of a rotor is developed appropriate for rotorcraft flight dynamic study and simulation in descent flight. The inflow model uses a series of vortex rings to create a nonlinear effect on rotor-induced velocity. Moreover, an augmentation to the total mass parameter in the existing inflow equation is suggested to create a steady-state transition between the helicopter and the windmill branches. With this inflow model, it is now plausible to predict rotor inflow over a wide range of descent rates.

Review of Momentum Theory

The steady-state normalized momentum equation for a rotor is given by [19]

$$\nu\sqrt{\bar{\mu}^2 + (\nu + \eta)^2} = 1 \tag{1}$$

For axial descent, it follows $\bar{\mu} = 0$. Equation (1) can then be simplified to the following form:

$$\nu^2(\nu + \eta)^2 = 1 \tag{2}$$

It follows that Eq. (2) can be solved for ν in terms of η.

$$\nu = \frac{-\eta + \sqrt{\eta^2 + 4}}{2}, \quad \forall\ \eta \tag{3}$$

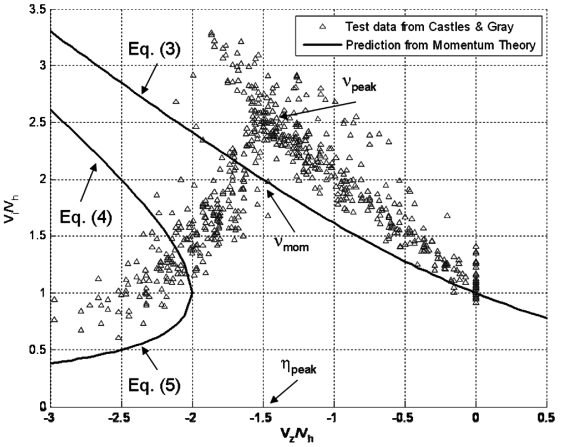

Fig. 1 Comparison between experimental data from Castles and Gray [1] and momentum theory.

$$\nu = \frac{-\eta + \sqrt{\eta^2 - 4}}{2}, \qquad \eta \le -2 \tag{4}$$

$$\nu = \frac{-\eta - \sqrt{\eta^2 - 4}}{2}, \qquad \eta \le -2 \tag{5}$$

Note that there are three solutions for ν when $\eta \le -2$. The preceding solutions of ν are plotted in Fig. 1. The upper branch corresponding to Eq. (3) is often called the helicopter branch, whereas the lower branch corresponding to Eq. (5) is the windmill branch.

Figure 1 also gives a comparison between the experimental data from [1] and the predictions from momentum theory. Three aspects of Fig. 1 are noteworthy. First, the momentum theory underpredicts the values of induced velocity along the helicopter and the windmill branches in descent flight. The increment of induced velocity from experimental data over the momentum theory prediction is clearly nonlinear. It is almost negligible at hover, but exhibits nonlinear characteristics with the increase of descent rates. The increment reaches its peak value at approximately $\eta = -1.5$. Second, experimental data shows a transition phase between the helicopter and the windmill branches. There is no such transition given by the momentum theory. Third, experimental data exhibit considerable fluctuation in the distribution of induced velocity. This feature is not captured by the momentum theory.

Ring Vortex Model

As indicated in [20], there is entrainment of air in the slipstream below the rotor and recirculation near the disk in descent condition. The effect of the interaction may be less significant at hover or in climb. Nevertheless, as a helicopter increases its descent rate, the interaction becomes more and more intense due to larger velocity gradients between the upflow outside the wake and the downflow inside the wake. Based on this observation, a simplified inflow model is proposed in [21] for a rotor in descent condition. This paper uses the ideas put forth in [21] in the development of a new inflow model called the ring vortex model (RVM).

Description of the RVM

In the RVM, flow around a rotor disk consists of slipstream and a series of discrete vortex rings along the wake at the rotor periphery due to flow interaction. Each vortex ring induces normal velocity at the rotor disk. The flowfield of a vortex ring can be computed based on elliptic integrals and its normal velocity components are tabulated in [22]. The combined effect between additional normal velocity from the vortex rings and the baseline induced velocity from the momentum theory provides an improvement in the prediction of inflow at the rotor disk in descent flight. One advantage of using

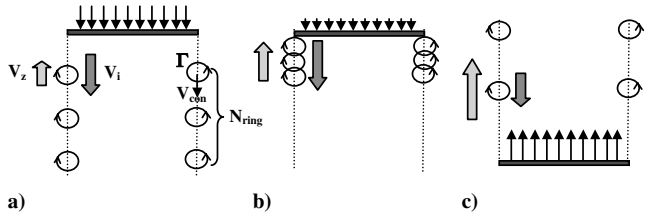

Fig. 2 Motion of vortex rings in axial descent: a) hover and slow descent, b) moderate rate of descent, and c) high rate of descent.

vortex rings is that its effect is nonlinear with respect to relative distance between the ring and the rotor disk. The closer a vortex ring is located to the rotor disk, the larger is its influence on the magnitude of normal velocity at the disk. Thus, the assumed nonlinear nature of induced velocity variation with descent rate conforms to the observation of experimental data shown in Fig. 1.

During axial descent, vortex rings move along the axial direction at the rotor periphery (a similar concept from Wang in [7]). The motion of the vortex rings depends on the rate of descent. As indicated in Fig. 2a, vortex rings move downward along the wake for axial descent at low rates. As the descent rate increases, vortex rings tend to accumulate near the rotor tip as shown in Fig. 2b. When the rate of descent further increases, vortex rings move upward along the wake as depicted in Fig. 2c. A new vortex ring is formed at every blade rotation, i.e., $2\pi/\Omega N_b$ s. The locations of these discrete vortex rings are determined by the product of convection velocity of the vortex rings and $2\pi m/\Omega N_b$ (where m is an integer representing the numbering of vortex rings).

Unlike axial descent, the flow environment in an inclined descent condition is no longer symmetric near the rotor disk [23]. From a modeling point of view, one needs to track relative distances between the aerodynamic computational points on the rotor blades and the vortex rings at every time step. Whereas some portions of the rotor disk experience downflow, other parts of the disk are subject to upflow. The resultant mean induced velocity is the average of induced velocities at different radial stations and azimuths.

In the following, important features of the RVM are illustrated in detail, including estimations of the convection speed of vortex rings, the vortex strength, and the number of vortex rings.

Convection Speed of Vortex Rings

It is observed from Fig. 1 that the increment of experimental data reaches its peak at a certain descent rate (approximately -1.5 in Fig. 1) in axial descent. In the RVM, the increment in induced velocity over momentum theory is caused by the presence of the vortex rings. Therefore, it can be reasoned that the vortex rings are located in the same plane of the rotor disk at $\eta = \eta_{\text{peak}}$. Thus, vertical convection speed of the vortex rings is close to zero at $\eta = \eta_{\text{peak}}$ to produce the largest increment in induced velocity at the rotor disk.

At hover, the vertical convection speed of the vortex rings is equal to V_h. Combining the convection speeds at both $\eta = 0$ and $\eta = \eta_{\text{peak}}$, the normalized vertical convection speed can be prescribed using the following formula:

$$\nu_{\text{ver,con}} = \upsilon - \frac{\upsilon_{\text{peak}}}{\eta_{\text{peak}}}\eta \tag{6}$$

Equation (6) represents, at best, a linear approximation of the actual convection speed of the vortex rings, which, perhaps, may be rather nonlinear.

In the inclined descent, the effect of forward velocity component is to sweep the vortex rings behind the rotor disk. Therefore, the convection speed of a vortex is the vector sum of vertical convection speed and forward velocity component.

$$\nu_{\text{con}} = \sqrt{\upsilon_{\text{com}}^2 + \bar{\mu}^2} \tag{7}$$

Vortex Strength and Number of Vortex Rings

In the previous study [21], the strength of vortex rings was assumed to be proportional to mean inflow velocity. Because vortex rings are produced due to entrainment of air between upflow outside the rotor wake and downflow inside the wake, the strength of vortex rings can be further assumed to be proportional to rotor radius as larger vortex rings trap more air. As such, the strength of a vortex ring may be estimated using

$$\Gamma = k_\Gamma R V_i \tag{8}$$

where k_Γ is a factor to be determined.

According to [22], the increment from the vortex rings is determined as

$$\Delta V_i = N_{\text{ring}} \frac{k_{\text{ring}}\Gamma}{R} \tag{9}$$

At $\eta = \eta_{\text{peak}}$, we have

$$\Delta V_i = (\upsilon_{\text{peak}} - \upsilon_{\text{mom}})V_h = N_{\text{ring}} \frac{k_{\text{ring}} k_\Gamma R \upsilon_{\text{peak}} V_h}{R} \tag{10}$$

A relationship between N_{ring} and strength factor k_Γ can thus be established by the following formula:

$$N_{\text{ring}} k_\Gamma = \frac{\nu_{\text{peak}} - \nu_{\text{mom}}}{k_{\text{ring}} \nu_{\text{peak}}} \tag{11}$$

The average value of k_{ring} is approximately 0.75 when a vortex ring is in the same plane of the rotor disk. If the values of ν_{peak} and ν_{mom} are known from the experiment, the product of N_{ring} and k_Γ becomes a constant. From Fig. 1, values for ν_{peak} and ν_{mom} are estimated to be roughly 2.5 and 2.0, respectively. It thus follows

$$N_{\text{ring}} k_\Gamma = 0.2667 \tag{12}$$

The actual number of vortex rings can be varied randomly within a specific range. With random variation of the number of vortex rings, magnitudes of induced velocities are expected to scatter around its nominal values. This provides a pattern of data fluctuation, which can be used to compare with data distribution from experiments. Furthermore, it provides a numerical means of simulating random fluctuations in rotor thrust and torque.

A sensitivity study was thus carried out to investigate the influence of the number of vortex rings in [24]. From Fig. 4 in [24], it is observed that the variation range of normalized induced velocity is more consistent with $N_{\text{ring}} = 2$ with a variation of the number of rings between zero and four. In the current study, the nominal number of vortex rings is thus taken as two.

Steady-State Transition

In the RVM, downward velocity is added to the induced velocity calculated from momentum theory. Nevertheless, in the current setting of momentum theory, there is no steady-state transition between the helicopter and the windmill branches for descent flight when $\bar{\mu} < 0.62$ [12]. As such, an augmentation to the total mass flow parameter in Eq. (1) is suggested by the insertion of an additional term:

$$\nu\sqrt{\left(\frac{\eta}{2.72(1+\bar{\mu}^2)}\right)^2 + \bar{\mu}^2 + (\eta+\nu)^2} = 1 \tag{13}$$

Figure 3 provides solutions of Eq. (13) for different values of normalized forward speed, V_x/V_h. With this additional term, equilibrium curves for inflow dynamics are modified, resulting in a smooth connection between the helicopter and the windmill branches in the inflow curve.

When $\eta + \nu = 0$ (ideal autorotation) and $\bar{\mu} = 0$ (axial descent), Eq. (13) has the solution $\eta = -\nu = -1.65$. Note that the experimental value for ideal autorotation is $\eta = -1.79$ [25,26]. The rational of such a selection is that -1.65 is the maximum value of

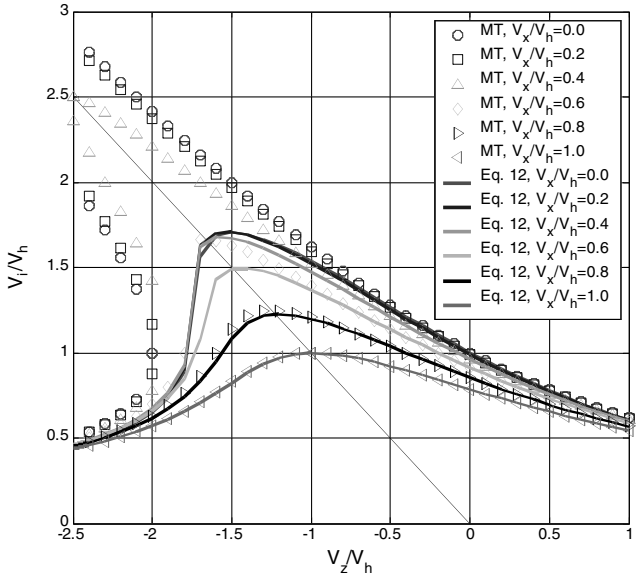

Fig. 3 Induced velocity variations with revised momentum theory (MT) from Eq. (12).

which Eq. (13) has no multiple equilibria over the entire range of descent rates. On the other hand, the difference between -1.65 and -1.79 can be easily compensated by the inclusion of vortex rings.

It is interesting to notice that the additional term

$$\left(\frac{\eta}{2.72(1+\bar{\mu}^2)}\right)^2$$

is proportional to η^2. In this sense, the term can be physically interpreted as a form of *parachute drag* because the rotor behaves like a parachute in the region of ideal autorotation.

When the rotor is in vertical climb, the value of ν reduces with the increase of climb rate. As such, Eq. (13) can be approximated by the following form

$$\nu\sqrt{\left(\frac{\eta}{2.72}\right)^2+\eta^2}=1 \tag{14}$$

Note that the influence of the term $(\eta/2.72)^2$ is much less than that of the term η^2. On the other hand, when the value of $\bar{\mu}$ is large

$$\left(\frac{\eta}{2.72(1+\bar{\mu}^2)}\right)^2 \ll \bar{\mu}^2$$

Therefore, it is concluded that the effect of the additional term diminishes in both climb and forward flight.

Finite-State Inflow Model

Simple momentum theory assumes a uniform induced velocity over the rotor disk. It cannot be used to investigate the effects of critical rotor parameters, like blade twist. A natural replacement is the finite-state inflow model [27]. Similar to the adjustment associated with simple momentum theory, the total mass flow parameter needs to be modified in a similar fashion to accommodate a steady-state transition between the helicopter and the windmill branches in the finite-state inflow model. Moreover, it is essential to include an appropriate number of inflow states for the intended study. In particular, a three-state inflow model is used for the sensitivity study related to radial variations (like blade twist), whereas a seven-state model can be used for the analysis related to both radial and azimuthal variations (for example, inclined descent). A formulation of the augmented three-state inflow model is provided in Appendix A. A step-by-step computation procedure for the RVM implementation is offered in Appendix B.

Test Data

A brief description of test data used for validation of the RVM is provided in the following.

Castles and Gray (1951)

Castles and Gray [1] performed wind tunnel tests for rotors operating in axial descent conditions. The basic rotor model had three blades with an effective solidity of 0.05 and NACA 0015 blade airfoil section. The tests were conducted at two different rotational speeds, 1200 and 1600 rpm. Four rotor configurations were tested: 1) constant-chord, untwisted blades of 6-ft-diam, 2) untwisted blades of 6-ft-diam, with a 3:1 taper, 3) constant-chord blades of 6-ft-diam, with a linear twist of -12 deg, and 4) constant-chord, untwisted blades of 4-ft-diam. Nevertheless, the tests were conducted in a 9 ft wind tunnel, indicating significant facility effect on the experimental results with a 6 ft rotor. Despite this concern, induced velocity data obtained in this test formed the basis of a variety of empirical inflow models (for example, [13,17]).

Yaggy and Mort (1962)

Yaggy and Mort [2] tested two vertical takeoff and landing propellers in descent flow condition. Of the two propellers, one was a conventional rigid propeller, and the other was an articulated (flapping only) propeller. Only the flapping propeller was considered in the subsequent RVM validation. The 9.5-m-diam propeller had a solidity of 0.203 and blade twist of -22.5 deg.

Washizu et al. (1966)

Washizu et al. [3] conducted moving track tests of a rotor in descent conditions. The 1.1-m-diam rotor had a solidity of 0.0573 and blade twist of -8.33 deg.

Taghizad et al. (2002)

ONERA (Taghizad et al. [13]) conducted flight tests in steep descents. The aircraft was an SA 365N Dauphin 6075 with a test weight of 3500 kg. The 11.2-m-diam main rotor had a solidity of 0.083 and blade twist of -10.2 deg.

RVM Model Validation Results and Discussion

In an effort to validate the RVM, six in-house rotor models and one full vehicle model were developed within the MATLAB^{TM} environment. Among the six rotor models, four correspond to different rotor configurations in Castles and Gray's tests [1], one for Yaggy and Mort's flapping propeller [2], and one for the rotor used by Washizu et al. [3]. Blade and rotor characteristics from those experiments are duplicated in the numerical simulation. Wind conditions are varied from each individual test. The blade element method was used for the analysis of aerodynamics. In addition, aerodynamic lift, drag, and pitch moment were calculated from two-dimensional airfoil table lookup. Moreover, three-state and seven-state inflow models were applied to the axial and inclined descent, respectively. Blade flapping motion was assumed to be quasi steady. In the case of the vehicle model, three translational motions as well as roll/pitch motions were modeled, although no yaw degree of freedom was included. In terms of RVM setup, the nominal number of vortex rings is taken to be two with $\eta_{\text{peak}}=-1.5$ and $\nu_{\text{peak}}=2.5$.

Induced Velocity in Axial Descent

Numerical studies are performed to compute induced velocity in axial descent for four different types of rotor models discussed in the earlier section. Results are presented in Figs. 4–8. In Figs. 6–8, results for axial flow are shown when $\alpha=90$ deg or $V_x/V_h=0.0$.

The mean induced velocity predictions with the RVM corresponding to four rotor configurations in Castles and Gray's [1] test are provided in Fig. 4. Different markers used in the figure represent a combination of thrust coefficient and rotor speed: unfilled markers stand for experimental data, whereas filled markers are predictions

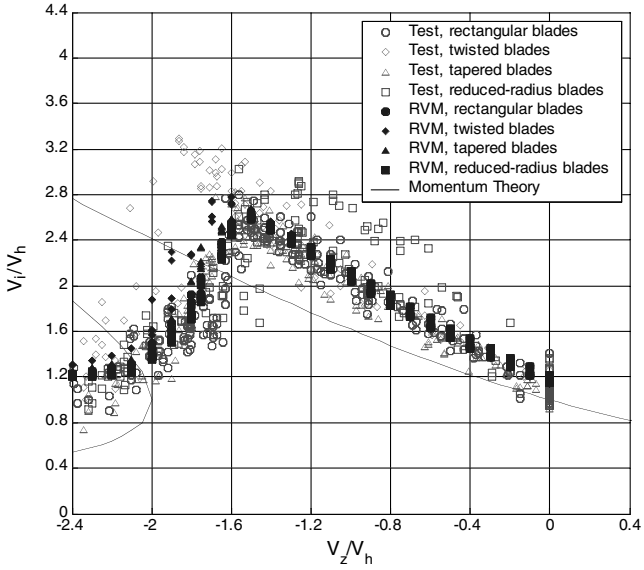

Fig. 4 Induced velocity variations from wind tunnel test [1] and predictions from the ring vortex model (axial flow).

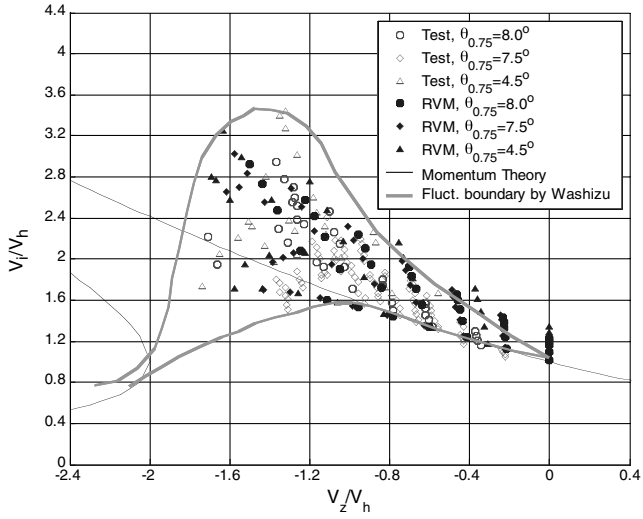

Fig. 5 Induced velocity variations from moving track test [3] and predictions from the ring vortex model (axial flow).

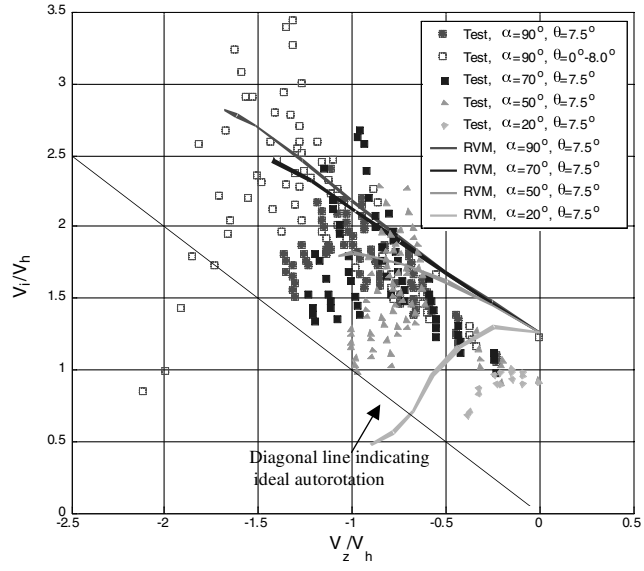

Fig. 6 . Induced velocity variations from moving track test [3] and predictions from the ring vortex model (axial and nonaxial flow).

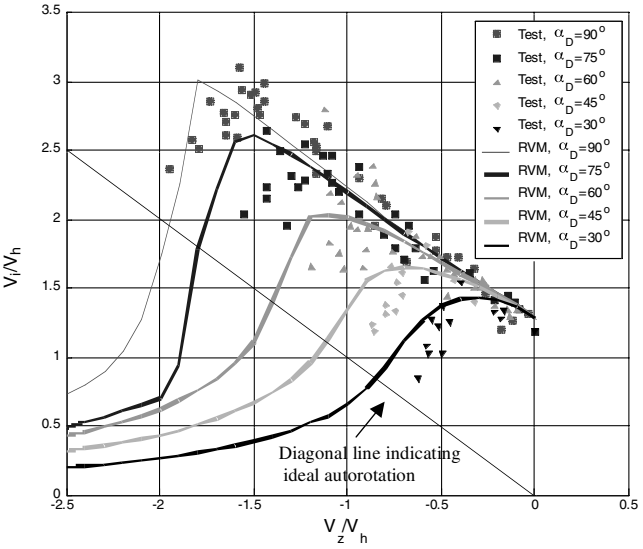

Fig. 7 Induced velocity variations from wind tunnel test [2] and predictions from the ring vortex model (axial and nonaxial flow).

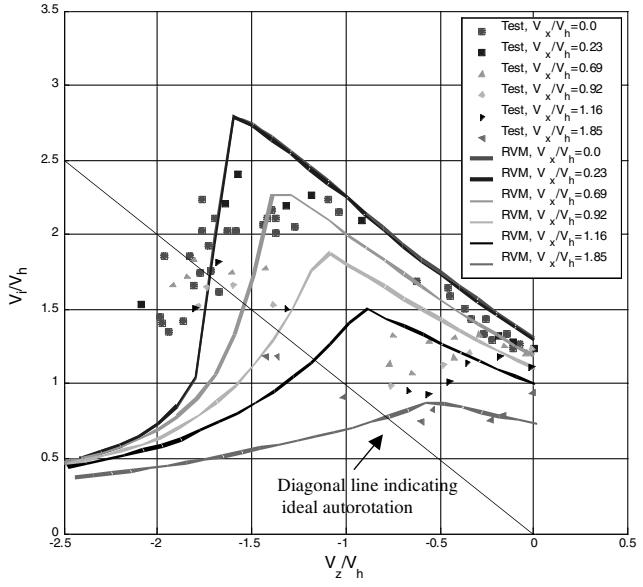

Fig. 8 Induced velocity variations from Dauphin flight test data [13] and predictions from the ring vortex model (axial and nonaxial flow).

using the RVM. Note that experimental data are not available for some combinations of thrust coefficient and rotor speed. From the comparison in Fig. 4, the mean induced velocity predictions from the RVM match well with averaged values from the test data, covering the range of descent rates from hover to $\eta = -2.4$. This indicates that the setting of nominal number of vortex rings to two is reasonable. One exception among four tested rotor configurations is the rotor with twisted blades. Whereas predictions from the RVM show peak induced velocity increased by 5% at a 7% higher descent rate due to blade twist, test data indicate a 24% increase at 17% higher descent rate. This discrepancy between the predictions and test data is further analyzed as part of the discussion on the effect of blade twist.

Heyson [28] compared the induced velocity results from both Castles and Gray [1] and Washizu et al. [3]. Although average values from [1,3] appeared to be consistent (see Figs. 4 and 5), the results from Washizu et al. [3] showed a wider variation of induced velocity. To investigate the scattered pattern of induced velocity in axial descent, the number of rings is allowed to vary from zero (without vortex rings) to four in Fig. 5. In the figure, induced velocities predicted with $N_{\text{ring}} = 0$ are close to the momentum theory and lower bound of the test data. With $N_{\text{ring}} = 2$, the calculated induced velocities tend to agree with the average values of the test data. The

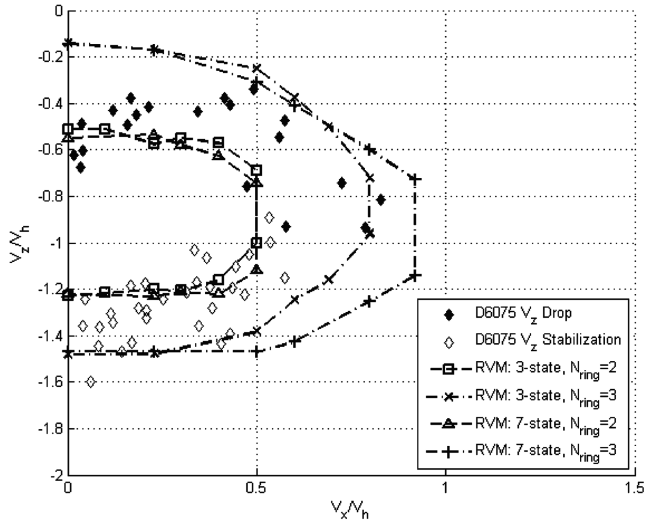

Fig. 9 Comparison of predicted VRS boundary with flight test results for Dauphin helicopter [13].

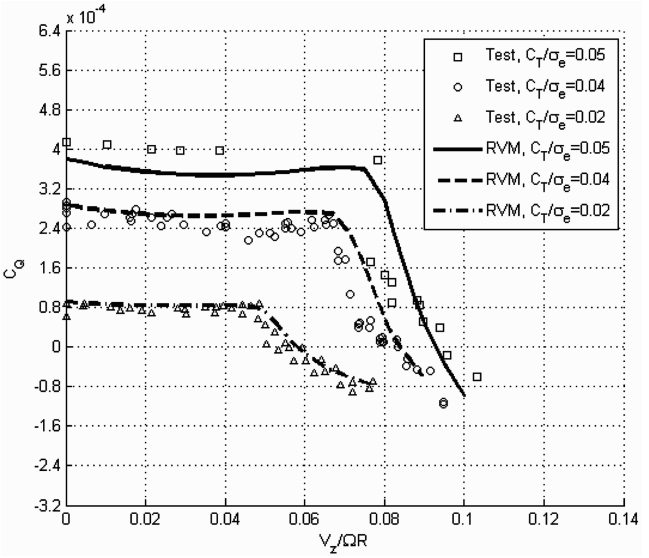

Fig. 10 Torque coefficient variation from wind tunnel test [1] and predictions from the ring vortex model (axial flow).

upper bound of scattered test data correlates well with the prediction using the RVM with $N_{\text{ring}} = 4$, especially over moderate descent rate. With a random number of vortex rings, the fluctuation pattern of induced velocities in Fig. 5 is in line with Heyson's finding [28].

Induced Velocity in Inclined Descent

Induced velocity comparisons in inclined descent are shown in Figs. 6–8. The rotor in the test by Washizu et al. [3] was at $\alpha = 70, 50,$ and 20 deg (Fig. 6), whereas the flapping propeller in Yaggy and Mort's [2] experiment was examined at $\alpha = 75$, 60, 45, and 30 deg (Fig. 7). Good agreement is seen between the predictions using the RVM and the averaged induced velocity data from both tests. It is noted that the predicted inflow curves in Fig. 6 are not extended to higher descent rates. This is because, at transition and windmill phases, it is difficult to numerically maintain high values of collective pitch settings in the steady-state sense.

Instead of maintaining constant descent angles in the tests by Washizu et al. [3] and Yaggy and Mort [2], forward speeds are kept constant in the Dauphin's flight test (Fig. 8) with V_x/V_h at 0.0, 0.23, 0.69, 0.92, 1.16, and 1.85. Generally, results from the RVM agree with the experimental data. At high forward speed ($V_x/V_h = 0.92$, 1.16, 1.85), predicted inflow curves from the RVM tend to get closer with simple momentum theory. In those conditions, vortex rings are further swept away from the rotor disk and their influence on rotor inflow is diminished. This suggests that the RVM is able to cover a wide range of descent flights at high advance ratios.

Prediction of VRS Stability Boundary

In the Dauphin flight test program [13], the crew would first feel an increase in vibration in the phase leading to VRS. This was followed by a sudden increase in the rate of descent. Increasing the collective would not prevent the helicopter from further descent. During the descent, the helicopter was very unstable and hard to control. The following criteria were used to arrive at the VRS boundary result in [13]: 1) sudden increase in the descent rate or vibration for entry into VRS, and 2) the pilot's ability to stabilize the rate of descent for exit out of VRS. Flight test results are shown in Fig. 9.

In the RVM prediction, there is not only an increase in the magnitude of induced velocity, but also a steeper and varying gradient of inflow curve [21,29]. This indicates that increase of induced velocity is more rapid than increase of descent rate. The direct impact of the steeper gradient is a change in sign of heave damping at certain descent rates as shown in [29]. Therefore, the descent rates for both VRS entry and exit can be determined by analyzing the gradient of inflow curves.

Using linearized models trimmed at different descent flight conditions, the heave mode stability is used as the criterion for arriving at the VRS boundary. During the computation, the nominal number of vortex rings in the RVM is chosen as two, whereas three vortex rings are considered as a worst case in the study. The results are shown in Fig. 9 together with flight test data. In the figure, smaller boundaries correspond to $N_{\text{ring}} = 2$, whereas larger boundaries match with $N_{\text{ring}} = 3$.

When $N_{\text{ring}} = 2$, the predicted VRS boundary appears circling around inner points of test data. When $N_{\text{ring}} = 3$, the corresponding VRS boundary embraces all the test points. A stability strip is created between these two boundaries. Within the strip, even if the heave mode is stable at one moment, it may become unstable at another moment due to random variation in the number of rings associated with the unsteady nature of flow in VRS.

In a broader view, the boundary with $N_{\text{ring}} = 3$ provides an advance warning to the helicopter at descent flight for potential VRS occurrence. The boundary with $N_{\text{ring}} = 2$ gives the most conservative (most severe) condition. Consequently, it is possible to design a VRS detection and avoidance system based on information from these two VRS boundaries.

The effect of the finite-state dynamic inflow model is also shown in Fig. 9. Two sets of VRS boundaries are given: one with three states (radial variation), and the other with seven states (radial and azimuthal variations). The seven-state model tends to expand the VRS boundary at relatively large forward speed. When the forward speed component is low, the boundaries are almost identical.

Power Increase During Descent

The rotor may consume more power at certain descent rates than at hover. Figure 10 shows torque coefficient as a function of descent rate with Castles and Gray's [1] baseline rotor configuration. It is observed that the rotor requires almost constant or more torque as descent rate increases from hover to a point when transition phase starts. In particular, when $C_T/\sigma_e = 0.05$, the required torque first decreases, and then increases in a region where thrust fluctuation normally occurs. The rotor torque finally decreases again as the rotor approaches transition and windmill phases.

Effect of Blade Twist

A study of blade twist is of particular interest as findings from past studies have been inconclusive in this regard. Castles and Gray [1] observed significant effect of blade twist in the wind tunnel test (see Fig. 4). Brown predicted that VRS boundary was sensitive to blade twist [11]. On the other hand, less significant effect from high blade twist was observed in defining the VRS boundary through the V-22 integrated test [14,15].

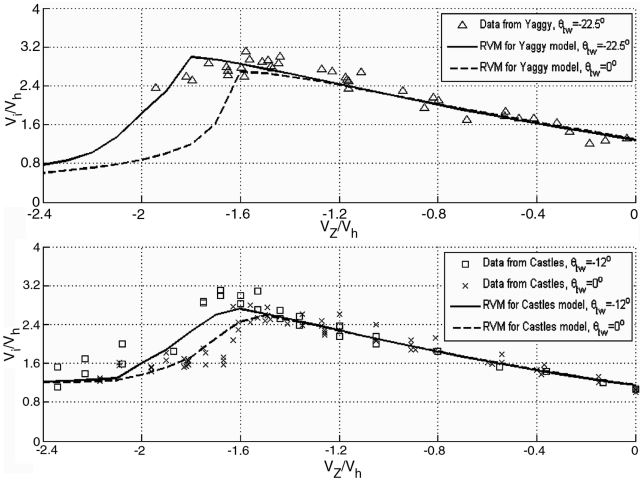

Fig. 11 Sensitivity study on blade twist.

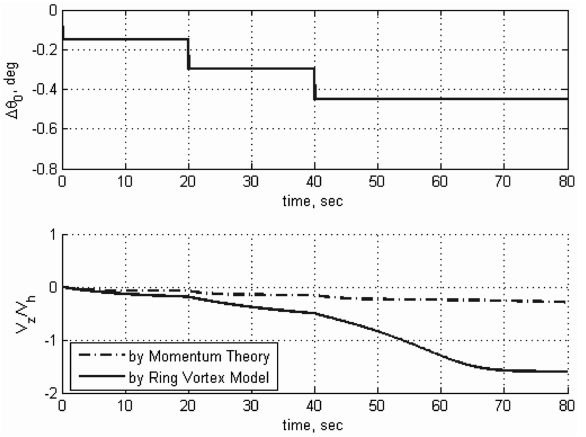

Fig. 12 Dynamic response of descent rate following moderate reduction in collective control.

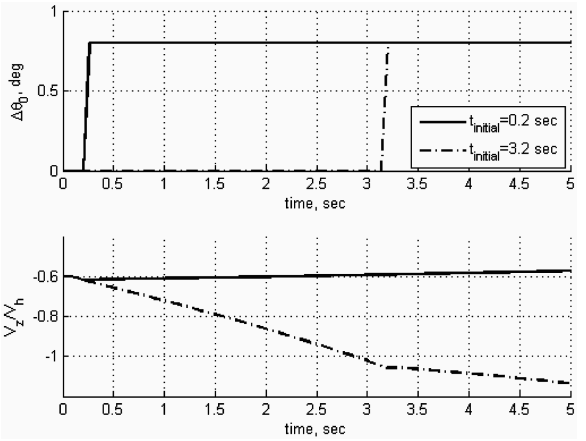

Fig. 13 Dynamic response of descent rate following increase of collective control initialized at different times.

To analyze the effect of blade twist, numerical studies are performed in terms of both Castles and Gray's [1] rotor model (blade twist of −12 deg) and Yaggy and Mort's [2] flapping propeller model (blade twist of −22.5 deg). Predictions from the RVM with and without blade twist are presented in Fig. 11. A higher rate of descent for ideal autorotation and higher v_{peak} at increased η_{peak} are observed in both cases in the presence of blade twist. The observations are in line with test results from Castles and Gray [1], although the differences with and without blade twist are less significant from the RVM. With higher blade twist in Yaggy and Mort's [2] experiment, these two effects appear to be stronger. This suggests that the RVM is able to reproduce these two effects due to blade twist and those effects tend to grow stronger as blade twist increases.

Effect of Other Rotor Parameters

Blade taper has a similar but less effect as blade twist on induced velocity distribution. Castles and Gray [1] suggest that it mainly increases the rate of descent for ideal autorotation by about 3% over the rotor with the blade with constant chord. The predicted increase from the RVM is about 3.55% for the same condition (Fig. 20 in [24]). Therefore, the effect of blade taper is captured well by the RVM.

Also from the numerical study of Castles and Gray's [1] rotor model, it is clear that there is no significant effect on the inflow curve with respect to rotor speed and rotor radius (Figs. 10–19 in [24]). This finding from the RVM is consistent with the conclusion from [1]. Therefore, it is possible to use a scaling technique (Froude scaling or Mach scaling) to enhance numerical reliability for small-scaled rotor models (including rotary wing unmanned aerial vehicles), as suggested in [29].

Dynamic Response with the RVM

Time simulations are conducted with an in-house rotorcraft flight dynamic model. Two cases are simulated. In the first case, the helicopter performs vertical descent from hover with designated collective reduction profile. The purpose is to qualitatively reproduce uncommanded drop of descent rate observed in the actual flight test. The second case involves vertical response of the vehicle following an increase of collective pitch initiated at different times. The objective is to identify the effectiveness of collective control in descent flight.

Results for the first simulation are shown in Fig. 12. In the top plot, the main-rotor collective pitch is reduced in steps from its trimmed value from hover. The reduction is small with a total collective change of −0.45 deg in 40 s. In the bottom plot, vertical responses are shown with inflow modeling based on momentum theory and the RVM. There is a clear contrast between these two vertical responses. With momentum theory, the change in vertical response of the helicopter due to the collective control change is moderate. At the end of the simulation, the descent rate reaches a steady-state value of $\eta = -0.3$. With the RVM, two moderate increases in descent rate can be first observed following the first two collective control reductions of 0.15 deg each. Following the third step reduction of 0.15 deg of collective (at $t = 40$ s), the descent rate of the vehicle goes through a significant change, indicating a loss of vertical damping as described in the previous section. The descent rate eventually reaches a steady-state value of $\eta = -1.6$.

Figure 13 shows response predictions from the second simulation. The helicopter is initially trimmed at $\eta = -0.6$ with the number of rings as two in the RVM. At $t = 0.1$ s, the number of vortex rings is changed to three, thus creating a situation of a reduction in rotor thrust due to an increase in induced velocity from the additional vortex ring. The resulting imbalance of vertical force on the vehicle causes its descent rate to increase. An increase in collective control (collective control pull) of 0.8 deg is initiated at different instances in time, i.e., at different values of descent rate, to arrest any further increase of the decent rate. The two collective control pull profiles used are shown in the top plot of Fig. 13. In the first case, the collective control pull starts at $t = 0.2$ s. The corresponding descent rate response shown in the bottom plot of Fig. 13 indicates that the collective control pull is able to arrest any further increase in the descent rate. In fact, with the collective control pull of 0.8 deg, the descent rate slightly decreases from its value at $t = 0.2$ s. This indicates that the pilot is still able to recover from the descent motion by pulling up the collective control. In the second case, the collective control pull is initiated at $t = 3.2$ s when the descent rate has already increased beyond $\eta = -1.0$. In this case, the descent rate continues to increase regardless of collective control increment. This result is in line with the observations from flight tests reported in [13].

Conclusions

A simplified inflow model, called the ring vortex model, is developed for a helicopter rotor in descent flight. The RVM consists of two parts. In the first part, a series of vortex rings are located along the rotor wake. Those rings induce additional downward velocity at the rotor disk, resulting in a nonlinear increase of induced velocity with descent rate, higher demands on the collective pitch and rotor power, and a significant change in the heave damping. In the second part, the inflow model from existing inflow models (momentum theory and finite-state inflow model) is modified to capture steady-state transition in the inflow curve between the helicopter and the windmill branches. Combining these two parts, it is now feasible to predict the inflow curve over a wide range of descent rates. Furthermore, thanks to its simple structure, the model can easily be implemented in flight mechanics codes to capture the helicopter's overall behavior in descent. Major conclusions from this study are summarized as follows:

1) The RVM appears to have good correlations of induced velocity and power required with test data over a wide range of descent rates. It is also able to capture the experimentally observed scatter in the induced velocity distribution.

2) The predicted VRS stability boundary using the RVM correlates well with the Dauphin's VRS boundary obtained from flight tests, especially with the inflow model covering both axial and azimuthal variations. Two contours are given corresponding to different numbers of vortex rings. The larger contour provides an advance warning to the helicopter for potential VRS occurrence, whereas the smaller one gives the most severe condition. Consequently, it is possible to design a VRS detection and avoidance system based on information from the predicted VRS boundary.

3) The effects of blade twist are shown in two aspects, including higher rate of descent for ideal autorotation and higher normalized peak induced velocity at increased normalized rate of descent. Within the range of the study (θ_{tw} from zero to -22.5 deg), the effects tend to grow stronger with the increased blade twist. These two aspects may just be part of the overall effects due to blade twist. A more extensive study is warranted for the side-by-side rotor configuration as it tends to have an even higher blade twist.

4) Prediction results using the RVM show insignificant effect from rotor speed and rotor radius. Therefore, it is possible to use scaling techniques to enhance numerical reliability in VRS studies.

5) Dynamic response predictions with the RVM demonstrate uncommanded drop in descent rate and loss of collective control effectiveness, two phenomena commonly observed for the single main-rotor helicopter in VRS.

Appendix A: Augmented Inflow Model

Augmented three-state inflow model [27]

$$M\dot{x} + L^{-1}\tilde{V}x = \tau \tag{A1}$$

where

$$M = \begin{bmatrix} 0.6366 & 0 & 0 \\ 0 & 0.2829 & 0 \\ 0 & 0 & 0.1811 \end{bmatrix} \tag{A2}$$

$$L^{-1} = \begin{bmatrix} 1.4694 & -0.4988 & 0.2274 \\ -0.4988 & 1.8624 & -0.6174 \\ 0.2274 & -0.6174 & 1.7591 \end{bmatrix} \tag{A3}$$

$$\tilde{V} = \begin{bmatrix} V_T & & \\ & V & \\ & & V \end{bmatrix} \tag{A4}$$

$$V_T = \sqrt{\left(\frac{\mu_z}{2.72(1+\bar{\mu}^2)}\right)^2 + \mu^2 + \lambda^2} \tag{A5}$$

$$V = \frac{\{\mu_z/[2.72(1+\overline{\mu}^2)]\}^2 + \mu^2 + (\bar{\lambda} + \bar{\lambda}_m)\bar{\lambda}}{\sqrt{\{\mu_z/[2.72(1+\overline{\mu}^2)]\}^2 + \mu^2 + \bar{\lambda}^2}} \tag{A6}$$

$$\bar{\lambda} = -\mu_z + \bar{\lambda}_m \tag{A7}$$

$$\bar{\lambda}_m = \frac{1}{2}\frac{\bar{C}_T}{\sqrt{\mu^2 + \bar{\lambda}^2}} \tag{A8}$$

The inflow state vector for radial variation with 0th harmonic is $x = [\alpha_1^0, \alpha_3^0, \alpha_5^0]^T$. The cosine pressure coefficient vector is $\tau = [\tau_1^{0c}, \tau_3^{0c}, \tau_5^{0c}]^T$. In addition, V_T and V are known as total flow parameter and flow parameter, respectively. The steady thrust coefficient is $\bar{C}_T$. More details of three-state (or an even higher state) inflow model can be found in [27].

Appendix B: Computation Procedure for the RVM Implementation

In this appendix, a step-by-step computational procedure with the ring vortex model is provided in the following:

1) Initialization.

2) Transform variables from body frame to hub frame.

3) Compute blade flapping angle (an example is given in [20]).

4) Obtain inflow state $\mathrm{x}_{\mathrm{old}}$ from initialization or replaced by $\mathrm{x}_{\mathrm{new}}$.

5) Compute induced velocity $\mathrm{w}_{i,j}$ from $\mathrm{x}_{\mathrm{old}}$ for ith blade at jth blade element from augmented inflow model (see Appendix A).

6) Compute convection speed and vortex strength [Eqs. (6–8)].

7) Compute $\Delta\nu_{i,j}$ with vortex rings, using table lookup from [22].

8) Compute combined normalized induced velocity, $\nu_{i,j} = \mathrm{w}_{i,j} + \Delta\nu_{i,j}$.

9) Compute blade local angle of attack.

10) Compute local c_l and c_d.

11) Compute sectional lift and drag.

12) Compute local normal, in-plane and radial forces.

13) Compute rotor thrust, H-force and Y-force.

14) Transformation from hub frame to tip path plane frame.

15) Compute $\mathrm{x}_{\mathrm{new}}$ from augmented inflow model (see Appendix A).

16) If $|\mathrm{x}_{\mathrm{new}} - \mathrm{x}_{\mathrm{old}}| < 0.01$, go back to step 4; otherwise, go to step 17

17) Compute rotor torque, pitching, and rolling moments

Acknowledgment

The first author would like to acknowledge the financial support from the Defence Science Organization National Laboratories, Singapore, for his graduate study program at the Georgia Institute of Technology.

References

[1] Castles, W., Jr., and Gray, R. B., "Empirical Relation Between Induced Velocity, Thrust, and Rate of Descent of a Helicopter Rotor as Determined by Wind Tunnel Tests on Four Model Rotors," NACA TN 2474, Oct. 1951.

[2] Yaggy, P. F., and Mort, K. W., "Wind Tunnel Tests of Two VTOL Propellers in Descent," NACA TN D-1766, March 1963.

[3] Washizu, K., Azuma, A., Koo, J., and Oka, T., "Experiments on a Model Helicopter Rotor Operating in the Vortex Ring State," *Journal of Aircraft*, Vol. 3, No. 3, May–June 1966, pp. 225–230.

[4] Wolkovitch, J., "Analytic Prediction of Vortex-Ring Boundaries for Helicopters in Steep Descents," *Journal of the American Helicopter*

Society, Vol. 17, No. 3, July 1971, pp. 13–19.

[5] Azuma, A., and Obata, A., "Induced Flow Variation of the Helicopter Rotor Operating in the Vortex Ring State," *Journal of Aircraft*, Vol. 5, No. 4, July–Aug. 1968, pp. 381–386.

[6] Empey, R. W., and Ormiston, R. A., "Tail-Rotor Thrust on a 5.5-foot Helicopter Model in Ground Effect," *American Helicopter Society Annual National Forum*, American Helicopter Society, Washington, D.C., May 1974.

[7] Wang, S. C., "Analytical Approach to the Induced Flow of a Helicopter Rotor in Vertical Descent," *Journal of the American Helicopter Society*, Vol. 35, Jan. 1990, pp. 92–98.

[8] Xin, H., and Gao, Z., "Experimental Investigation of Model Rotors Operating in Vertical Descent," *19th European Rotorcraft Forum*, Sept. 1993.

[9] Xin, H., and Gao, Z., "Prediction of the Vortex-Ring State Boundary Based on Model Tests," *Transactions of Nanjing University of Aeronautics and Astronautics*, Vol. 11, No. 2, Dec. 1994, pp. 159–164.

[10] Leishman, J. G., Bhagwat, M. J., and Ananthan, S., "Free-Vortex Wake Predictions of the Vortex Ring State for Single-Rotor and Multi-Rotor Configurations," *American Helicopter Society 58th Annual Forum, Montréal, Canada, June 11–13, 2002*, American Helicopter Society, Alexandria, VA, 2002.

[11] Brown, R. E., Leishman, J. G., Newman, S. J., and Perry, F. J., "Blade Twist Effects on Rotor Behavior in the Vortex Ring State," *28th European Rotorcraft Forum, Bristol, England*, 2002.

[12] Basset, P. M., and Prasad, J. V. R., "Study of the Vortex Ring State Using Bifurcation Theory," *American Helicopter Society 58th Annual Forum, Montréal, Canada, June 11-13, 2002*, American Helicopter Society, Alexandria, VA, 2002.

[13] Taghizad, A., Jimenez, J., Binet, L., and Heuzé, D., "Experimental and Theoretical Investigation to Develop a Model of Rotor Aerodynamics Adapted to Steep Descent," *American Helicopter Society 58th Annual Forum, Montréal, Canada, June 11–13, 2002*, American Helicopter Society, Alexandria, VA, 2002.

[14] Brand, A., Kisor, R., Blyth, R., Mason, D., and Host, C., "V-22 High Rate of Descent (HOD) Test Procedures and Long Record Analysis," *American Helicopter Society 60th Annual Forum, Baltimore, Maryland, June 7–10, 2004*, American Helicopter Society, Alexandria, VA, 2004.

[15] Kisor, R., Blyth, R., Brand, A., and MacDonald, T., "V-22 Low-Speed/High Rate of Descent (HROD) Test Results," *American Helicopter Society 60th Annual Forum, Baltimore, Maryland, June 7–10, 2004*, American Helicopter Society, Alexandria, VA, 2004.

[16] Glauert, H., "Analysis of Experimental Results in the Windmill Bake and Vortex Ring States of an Airscrew," R. & M. No. 1026, British Aeronautical Research Council, 1926.

[17] He, C. J., Lee, C. S., Chen, W. B., "Finite State Induced Flow Model in Vortex Ring State," *Journal of the American Helicopter Society*, Vol. 45, No. 4, Oct. 2000, pp. 318–320.

[18] Johnson, W., "Model for Vortex Ring State Influence on Rotorcraft Flight Dynamics," *AHS 4th Decennial Specialist's Conference on Aeromechanics, San Francisco, California, January 21–23, 2004*, American Helicopter Society, Alexandria, VA, 2004.

[19] Peters, D. A., and Chen, S. Y., "Momentum Theory, Dynamic Inflow, and the Vortex Ring State," *Journal of the American Helicopter Society*, Vol. 28, No. 3, July 1982, pp. 18–24.

[20] Johnson, W., *Helicopter Theory*, Princeton Univ. Press, Princeton, NJ, 1980, pp. 98–102.

[21] Chen, C., Prasad, J. V. R., and Basset, P. M., "Simplified Inflow Model of a Helicopter Rotor in Vertical Descent," *American Helicopter Society 60th Annual Forum, Baltimore, Maryland, June 7–10, 2004*, American Helicopter Society, Alexandria, VA, 2004.

[22] Castles, W., and Leeuw, J. H., "The Normal Component of the Induced Velocity in the Vicinity of a Lifting Rotor and Some Examples of its Application," NACA TN 2912, 1953.

[23] Chen, C., and Prasad, J. V. R., "Simplified Inflow Model of a Helicopter Rotor in Forward Descent," *43rd AIAA Aerospace Sciences Meeting and Exhibit, Reno, Nevada, Jan 10–13, 2005*, AIAA, Reston, VA, 2005.

[24] Chen, C., and Prasad, J. V. R., "Ring Vortex Model for Descent Flight," *American Helicopter Society 61st Annual Forum, Grapevine, Texas, June 1–3, 2005*, American Helicopter Society, Alexandria, VA, 2005.

[25] Prouty, R. W., "Helicopter Performance, Stability, and Control," Krieger, Malabar, FL, 1986, pp. 109–115.

[26] Padfield, R. W., *Helicopter Flight Dynamics*, Blackwell Science, Boston, MA, 1996, pp. 115–118.

[27] He, C. J., "Development and Application of a Generalized Dynamic Wake Theory for Lifting Rotors," Ph.D. Dissertation, Georgia Inst. of Technology, School of Aerospace Engineering, Aug. 1989.

[28] Heyson, H. H., "Momentum Analysis of Helicopters and Autogyros in Inclined Descent, with Comments on Operational Restrictions," NASA TN D-7917, Oct. 1975.

[29] Prasad, J. V. R., Chen, C., Basset, P. M., and Kolb, S., "Simplified Model and Nonlinear Analysis of a Helicopter Rotor in Vortex Ring State for Flight Simulation," *30th European Rotorcraft Forum, Marseilles, France*, 2004.